Results in Physics 8 (2018) 379–390

Contents lists available at ScienceDirect

Results in Physics

journal homepage: www.journals.elsevier.com/results-in-physics

Application of discontinuous Galerkin method for solving a compressible five-equation two-phase flow model

M. Rehan Saleem [a,*], Ishtiaq Ali [a], Shamsul Qamar [a,b]

[a] COMSATS Institute of Information Technology, Park Road, Chak Shahzad Islamabad, Pakistan
[b] Max Planck Institute for Dynamics of Complex Technical Systems, Magdeburg, Germany

ARTICLE INFO

Article history:
Received 20 October 2017
Received in revised form 11 December 2017
Accepted 15 December 2017
Available online 21 December 2017

Keywords:
Two-phase compressible flows
Non-conservative system
Shock discontinuities
Discontinuous Galerkin method
Central scheme

ABSTRACT

In this article, a reduced five-equation two-phase flow model is numerically investigated. The formulation of the model is based on the conservation and energy exchange laws. The model is non-conservative and the governing equations contain two equations for the mass conservation, one for the over all momentum and one for the total energy. The fifth equation is the energy equation for one of the two phases that includes a source term on the right hand side for incorporating energy exchange between the two fluids in the form of mechanical and thermodynamical works. A Runge-Kutta discontinuous Galerkin finite element method is applied to solve the model equations. The main attractive features of the proposed method include its formal higher order accuracy, its nonlinear stability, its ability to handle complicated geometries, and its ability to capture sharp discontinuities or strong gradients in the solutions without producing spurious oscillations. The proposed method is robust and well suited for large-scale time-dependent computational problems. Several case studies of two-phase flows are presented. For validation and comparison of the results, the same model equations are also solved by using a staggered central scheme. It was found that discontinuous Galerkin scheme produces better results as compared to the staggered central scheme.

Introduction

In two-phase flows, two fluids of different densities are separated by a thin interface (see Fig. 1). The flow can be incompressible or compressible. Phases are identified as "homogeneous" parts of the fluid for which unique local state and transport properties can be defined. Generally, phases are considered as the state of matter, e.g. gas/vapor, liquid, or solid. The flow of gas carrying liquid droplets or solid particles or the flow of liquid carrying vapor or flow of solid granular material and fluid or gas bubbles are the typical examples of two-phase flows. Normally, in the case of two-phase flows, we are not interested in a detailed description of particle interaction, instead we want to describe the flow as a whole. This is exactly the situation where the homogenized approach comes into play. An important issue concerning the systems of governing equations for two-phase flow models is that they are intrinsically non-conservative. The mathematical structures of the non-conservative systems are more complicated as compared to conservation laws. Also, there is a lack of theory for numerical methods to solve such systems. On the other hand, the development of efficient numerical methods for the solution of two-phase flows is of great importance. As the model equations are intrinsically non-conservative, one has to provide non-conservative methods for their solutions.

Two phase flows can be observed in nature very easily, such as rainy or snowy winds, avalanches, debris flows, tornadoes, typhoons, air and water pollution, volcanic activities, and so on. They are also working processes in a variety of conventional and nuclear power plants, combustion engines, propulsion systems, oil and gas transport, chemical industry, biological industry, process technology in the metallurgical industry or in food production, blood flow, and etc. Due to their wide range applications, two-phase flows require suitable mathematical models to predict their physical behavior. However, modeling and simulation of such flows are challenging tasks.

Methods of averaging have been in use since the mid-70s when Ishii [1] presented the governing equations for the homogenized flow in his classical book. Nowadays, the more or less established basic model includes the two continuity, two momentum, and two energy equations for both phases. The averaging of the single phase equations results in additional terms, which describe the

* Corresponding author.
E-mail address: muhammad.rehan@iiu.edu.pk (M.R. Saleem).

https://doi.org/10.1016/j.rinp.2017.12.044
2211-3797/

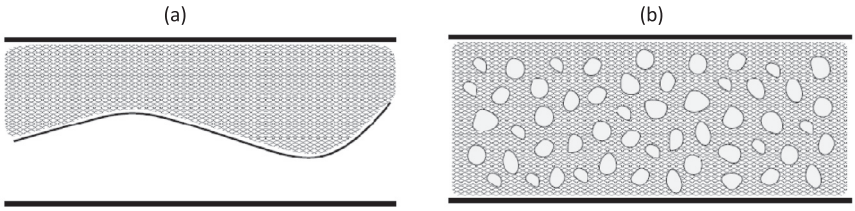

Fig. 1. Schematic diagram for two types of flows. (a) Flows separated by sharp interface. (b) Multiphase flows.

interaction between the phases. These are the mass transfer terms for the continuity equations, the momentum exchange terms for the momentum equations, and the energy exchange terms for the energy equations. The closure to the system of governing equations is usually achieved by adding an additional equation for the fraction of one of the phases, and the equations of state for both phases. Another approach is to use some simplifying assumptions, like incompressibility of one phase, equality of pressures, and etc.

Several two-phase flow models exist in the literature for describing the behavior of physical mixtures. For each fluid, they contain separate pressures, velocities and densities. If a convection equation for the interface motion is coupled with the conservation laws, the models are called as seven-equation models. One of such models for solid-gas two-phase flows was initially introduced by Baer and Nunziato [2] and it was further investigated by Abgrall and Saurel [3,4]. These seven equation models are considered as the best and established two-phase flow models. However, they have a number of numerical complexities. To resolve these difficulties researchers have proposed reduced three to six-equation models [5–7].

Kapila deduced a five equation model [5] from Baer and Nunziato's seven-equation model [2] and it is a well known reduced model that has been successfully implemented to study interfacing compressible fluids, barotropic and non-barotropic cavitating flows. The Kapila's five-equation model contains first four conservative equations, two for the mass conservation of both fluids, one for the total momentum conservation of the mixture and one for the total energy conservation. The fifth equation is a non-zero convection equation for the volume fraction of one of the two phases.

Although, Kapila's five equation model is simple, but it has a number of serious difficulties. For example, the model is still non-conservative and, thus, it is difficult to obtain a numerical solution which converges to the physical solution. Another issue is related to non-conservative behavior of the mixture sound speed [8].

In order to make the Kapila's five-equation model easier and to remove the aforementioned difficulties, Kreeft and Koren [6] have introduced a new formulation of the Kapila's five equation model. This new model is also non-conservative and it contains five equations [6]. The first two equations are for the conservation of mass, one for the mixture momentum conservation and one for the total energy conservation. The fifth equation is the energy equation for one of the two phases which includes a source term on the right hand side representing the energy exchange between two fluids in the form of mechanical and thermo-dynamical work. The two-phase flow models have already been solved by finite volume type schemes, such as central upwind scheme, central NT scheme, space-time CESE scheme and kinetic flux vector splitting (KFVS) scheme [9–13]. Also, diffuse interface method and finite volume WENO scheme have been used to solve the two-phase flow models [14–16].

The discontinuous Galerkin (DG) finite element method was initially introduced by [17] for solving neutron transport equations. Afterwards, various DG methods were developed and formulated by Cockburn and Shu for nonlinear hyperbolic system in the series of papers, see for example [18–20]. DG-methods are being applied in the main stream of computational fluid dynamic models, see for example [21–25]. The DG methods are versatile, flexible, and have intrinsic stability making them suitable for convection dominated problems. DG-methods can be efficiently applied to partial differential equations (PDEs) of all kind including equations whose type changes within the computational domain.

DG-methods belong to the class of finite element method (FEM) which have several advantages over finite difference methods (FDMs) and finite volume methods (FVMs). For instance, they inherit geometric flexibility of FVMs and FEMs, retain the conservation properties of FVMs, and possess high-order properties of FEMs. Therefore, DG-methods are locally conservative, stable, and high order accurate. These methods satisfy the total variation bounded (TVB) property that guarantees the positivity of the schemes, see e.g. [18–20]. In contrast to high order FDMs and FVMs, DG-methods require a simple treatment of the boundary conditions in order to achieve high order accuracy uniformly. Moreover, DG methods allow discontinuous approximations and produce block-diagonal mass matrices that can be easily inverted through algorithms of low computational cost. These methods incorporate the idea of numerical fluxes and slope limiters in a very natural way to avoid spurious oscillations (wiggles), which usually occur due to shocks, discontinuities or sharp changes in the solution.

In this paper, Runge-Kutta DG-scheme of order two is implemented for solving the reduced five-equation model of Kreeft and Koren [6,18–20]. The scheme employs a DG-method in the space-coordinate that converts the given system of partial differential equations to a system of ordinary differential equations (ODEs). The resulting ODE-system is then solved by using explicit and nonlinearly stable high order Runge-Kutta method. To guarantee the positivity of the numerical scheme an additional TVB property of the proposed ODE-solver along with the RK-DG is used. The numerical test problems of this manuscript verify the accuracy and efficiency of the current DG-scheme for solving two-phase flow models. For validation, the numerical results of the proposed scheme are compared with those obtained from the staggered central NT scheme [26].

The present article is organized as follows. Section "Compressible two-phase flow model" is devoted to the introduction of one-dimensional compressible two-phase flow model of Kreeft and Koren [6]. The discontinuous Galerkin method is presented in Section "Discontinuous Galerkin method for compressible TPSF model". Numerical case studies are carried out in Section "Numerical test problems". Finally, concluding remarks are given in Section "Conclusions".

Compressible two-phase flow model

In this section, the one-dimensional reduced two-phase flow model of Kreeft and Koren [6] is presented. The considered model

is the reformulation of original five-equation model of Kapila et al. [5]. In this model, it is assumed that the mass of both fluids is conservative and both fluids have the same velocity and pressure on either sides of the sharp interface. Moreover, the effects of heat conduction and viscosity are not considered in this model. In the current model, the first four equations are for the conservative quantities: two for the mass, one for the over all momentum and one for the total energy. The fifth one is the energy equation that includes the source term on the right side describing energy exchange between the two fluids in the form of mechanical and thermodynamical work. The state vector $\mathbf{q}$ for the primitive variables has the form $\mathbf{q} = (\rho, \mathbf{u}, p, \alpha)^T$, where the density of mixture is denoted by ρ, the bulk velocities along each characteristic direction are $\mathbf{u} = (u, 0, 0)$, p represents the bulk pressure and α denotes the volume fraction of fluid 1. It shows that a part α of a small volume dV is filled with fluid 1 and a part $(1-\alpha)$ with fluid 2.

For bulk quantities, such as mixture density ρ and mixture total energy E, we assume that α is a volume fraction of fluid 1 and $(1-\alpha)$ of fluid 2. Using these conventions, we can define

$$\rho = \alpha\rho_1 + (1-\alpha)\rho_2, \quad \rho E = \alpha\rho_1 E_1 + (1-\alpha)\rho_2 E_2 \tag{1}$$

and the total energies of each fluid as

$$E_1 = e_1 + \frac{1}{2}u^2, \quad E_2 = e_2 + \frac{1}{2}u^2, \tag{2}$$

where e_1 and e_2 are the internal energies of fluid 1 and fluid 2, respectively. The internal energies e_1 and e_2 are given in terms of their respective densities and pressure through equations of state

$$e_1 = e_1(\rho_1, p), \quad e_2 = e_2(\rho_2, p). \tag{3}$$

In the one dimensional form, the two-phase flow model can be written as [6]

$$\mathbf{w}_t + \mathbf{f}(\mathbf{w})_x = \mathbf{s}(\mathbf{w}), \tag{4a}$$

where

$$\mathbf{w} = (\rho, \rho u, \rho E, \rho_1\alpha, \rho_1 E_1\alpha)^T, \tag{4b}$$

$$\mathbf{f}(\mathbf{w}) = \left(\rho u, \rho u^2 + p, \rho u E + p u, \rho_1 u\alpha, \rho_1 E_1 u\alpha + p u\alpha\right)^T, \tag{4c}$$

$$\mathbf{s}(\mathbf{w}) = (0, 0, 0, 0, s_5)^T. \tag{4d}$$

Here, $\mathbf{w}$ denotes the vector of conserved variables, $\mathbf{f}$ represents the vector of fluxes, $\mathbf{s}$ is a vector of source terms with only last term as non-zero. The last term of source vector s_5 represents the total rate of energy exchange per unit volume between fluid 1 and fluid 2 and is equal to the sum of rates of mechanical s_5^M and thermodynamic s_5^T works [6], i.e. $s_5 = s_5^M + s_5^T$, with

$$s_5^M = u(p\alpha)_x - \beta u p_x, \tag{5}$$

$$s_5^T = p\alpha(1-\alpha)\frac{\tau_2 - \tau_1}{\tau}u_x. \tag{6}$$

The term $\beta = \frac{\rho_1\alpha}{\rho}$ denotes the mass fraction of fluid 1, while the relations $\tau_1 = \frac{1}{\rho_1 c_1^2}$ and $\tau_2 = \frac{1}{\rho_2 c_2^2}$ denote the isentropic compressibilities of fluid1 and fluid 2. Here, c_1 and c_2 are the sound speeds of both fluids. The bulk isentropic compressibility is defined as

$$\tau = \alpha\tau_1 + (1-\alpha)\tau_2. \tag{7}$$

Assume that the equations of state in Eq. (3) are the stiffened equations of state [6]

$$\rho_i e_i = \frac{p + \pi_i\gamma_i}{\gamma_i - 1}, \quad i = 1, 2, \tag{8}$$

where γ_i, π_i are the material specific quantities. The sound speeds in each fluid are given as

$$c_i = \sqrt{\frac{(p+\pi_i)\gamma_i}{\rho_i}}, \quad i = 1, 2. \tag{9}$$

The expressions for the sound speeds are normally obtained from the second law of thermodynamics. The total energies of fluids 1 and 2 can be given as

$$\rho_1 E_1\alpha = \frac{p + \pi_1\gamma_1}{\gamma_1 - 1}\alpha + \frac{1}{2}\rho_1\alpha u^2, \tag{10}$$

$$\rho_2 E_2(1-\alpha) = \frac{p + \pi_2\gamma_2}{\gamma_2 - 1}(1-\alpha) + \frac{1}{2}(\rho - \rho_1\alpha)u^2. \tag{11}$$

Using Eqs. (4), (10) and (11), we obtained the primitive variables as

$$\rho = w_1, \quad u = \frac{w_2}{w_1}, \tag{12}$$

$$\alpha = \begin{cases} \frac{\beta_1}{\beta_1+\beta_2}, & \text{if } \pi_1 = 0 = \pi_2, \\ \frac{\pi_2\gamma_2 - \pi_1\gamma_1 - \beta_1 - \beta_2 \pm \sqrt{(\pi_2\gamma_2 - \pi_1\gamma_1 - \beta_1 - \beta_2)^2 + 4\beta_1(\pi_2\gamma_2 - \pi_1\gamma_1)}}{2(\pi_2\gamma_2 - \pi_1\gamma_1)}, & \text{otherwise}, \end{cases} \tag{13}$$

$$p = \beta_1 + \beta_2 - \alpha\pi_1\gamma_1 - (1-\alpha)\pi_2\gamma_2, \tag{14}$$

where

$$\beta_1 = (\gamma_1 - 1)\left(w_5 - \frac{w_4(w_2^2)}{2w_1^2}\right), \tag{15}$$

$$\beta_2 = (\gamma_2 - 1)\left(w_3 - w_5 - \frac{(w_1 - w_4)(w_2^2)}{2w_1^2}\right). \tag{16}$$

Here, $w_i;\ i = 1, \ldots, 5$, denote the components of $\mathbf{w}$, the vector of conserved variables. Furthermore, in Eqs. (12)–(14) the primitive variables are expressed in terms of conserved variables. Eq. (13) takes the upper positive sign when $(\pi_2\gamma_2 - \pi_1\gamma_1) > 0$ and lower negative sign otherwise. Using the values of c_1 and c_2 from Eq. (9), we obtain the following expressions for τ_1 and τ_2.

$$\tau_1 = \frac{1}{\rho_1 c_1^2} = \frac{1}{(p+\pi_1)\gamma_1}, \quad \tau_2 = \frac{1}{\rho_2 c_2^2} = \frac{1}{(p+\pi_2)\gamma_2}. \tag{17}$$

Eigen-values of the model

The quasi-linear form of the Eq. (4) is given by

$$\frac{\partial\mathbf{w}}{\partial t} + A(\mathbf{w})\frac{\partial\mathbf{w}}{\partial x} = \mathbf{s}(\mathbf{w}), \tag{18}$$

where A($\mathbf{w}$) is the Jacobian matrix for the system under investigation and is given by the following matrix

$$A(\mathbf{w}) = \begin{pmatrix} u & \rho & 0 & 0 & 0 \\ 0 & u & 1/\rho & 0 & 0 \\ 0 & \rho c^2 & u & 0 & 0 \\ 0 & 0 & 0 & u & 0 \\ 0 & \Psi & 0 & 0 & u \end{pmatrix}. \tag{19}$$

where Ψ is given by the following relation

$$\Psi = \alpha(1-\alpha)\frac{\tau_2 - \tau_1}{\tau}.$$

Moreover, τ_1, τ_2 and c_1, c_2 are given in Eq. (17) and Eq. (9), respectively. We obtain three distinct eigen-values for the jacobian matrix A($\mathbf{w}$). Hence, this 1D system is hyperbolic with wave speeds given by

$$\lambda_1 = u - c, \quad \lambda_{2,3,4} = u, \quad \lambda_5 = u + c. \tag{20}$$

A finite element which contains the both fluids, has a single speed of sound c as the bulk speed of sound.

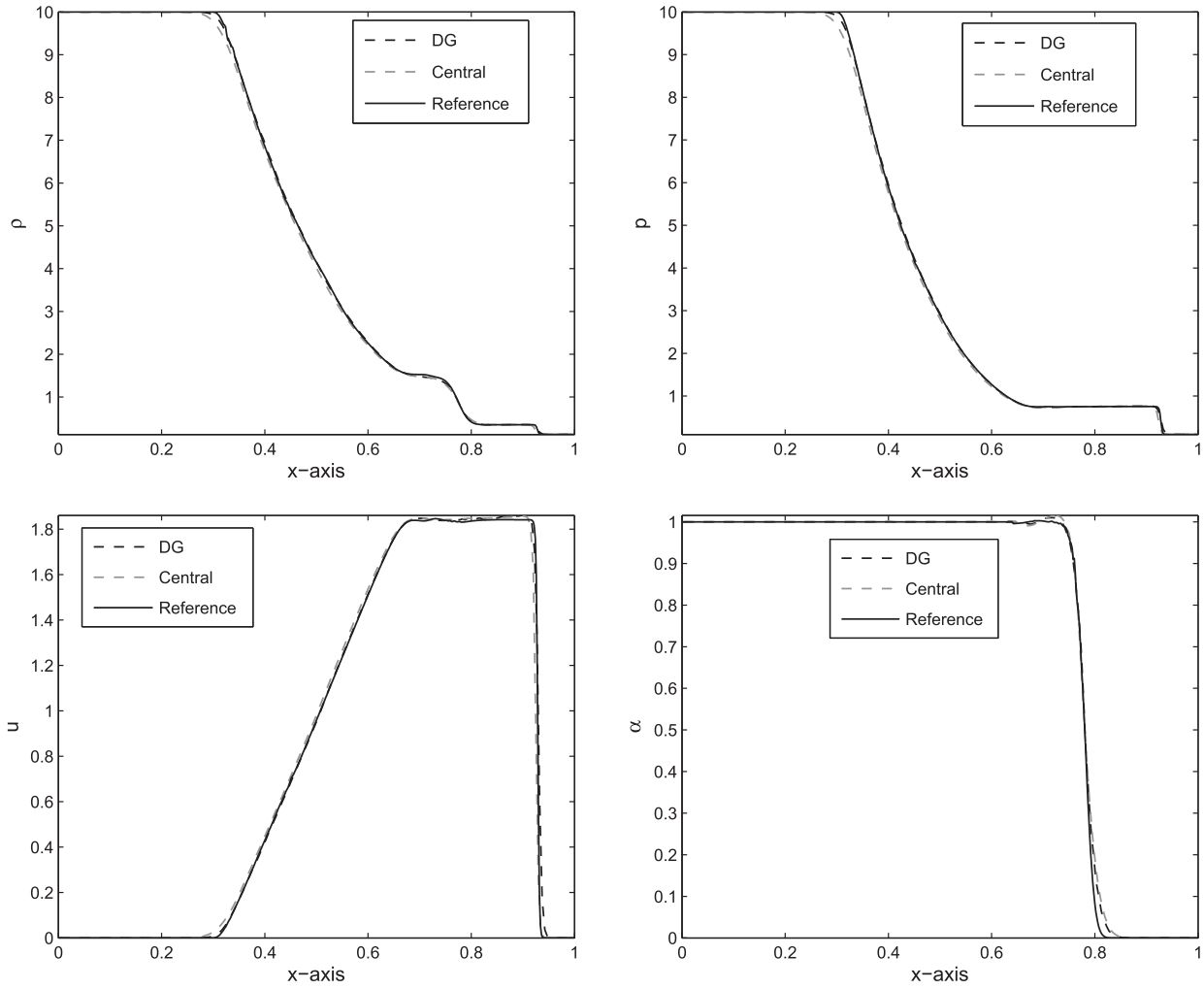

Fig. 2. Comparison of DG and central NT schemes for Sod's Problem 1 at time $t = 0.15$.

Table 1
Comparison of L^1-errors for Problem 1.

N	Density (ρ)		Volume fraction (α)		Pressure (p)		Velocity (u)	
	DG	Central	DG	Central	DG	Central	DG	Central
100	0.062	0.182	0.013	0.017	0.026	0.077	0.024	0.077
200	0.026	0.081	0.006	0.008	0.024	0.057	0.010	0.032
300	0.024	0.052	0.004	0.005	0.023	0.049	0.010	0.020
400	0.021	0.029	0.002	0.003	0.019	0.029	0.010	0.011
500	0.019	0.019	0.001	0.002	0.017	0.022	0.007	0.009

Discontinuous Galerkin method for compressible TPSF model

In this section, the proposed DG-method is applied to the aforementioned one-dimensional compressible two-fluid flow model. In one space dimension, two-fluid flow model in Eq. (4) reduces to:

$$\frac{\partial \mathbf{w}}{\partial t} + \frac{\partial \mathbf{f}(\mathbf{w})}{\partial x} = \mathbf{s}(\mathbf{w}), \tag{21}$$

where

$$\mathbf{w} = (\rho, \rho u, \rho E, \rho_1 \alpha, \rho_1 E_1 \alpha)^T, \tag{22}$$

$$\mathbf{f}(\mathbf{w}) = (\rho u, \rho u^2 + p, \rho u E + p u, \rho_1 u \alpha, \rho_1 E_1 u \alpha + p u \alpha)^T, \tag{23}$$

$$\mathbf{s}(\mathbf{w}) = (0, 0, 0, 0, s_5)^T. \tag{24}$$

Here, the DG-scheme [18–20,27,28] is implemented for the discretization of space-coordinate only. The derivatives of time coordinate are discretized by using the TVB Runge-Kutta method.

In order to discretize the spatial domain $[x_0, x_{\max}]$, we proceed as follows. For $j = 0, 1, 2, \ldots .N$, let $x_{j+\frac{1}{2}}$ be the cells partitions, $I_j = \left(x_{j-\frac{1}{2}}, x_{j+\frac{1}{2}}\right)$ be the domain of cell j, $\Delta x_j = x_{j+\frac{1}{2}} - x_{j-\frac{1}{2}}$ be the width of cell j, and $I = UI_j$ be the union of partitions in the whole domain. We seek an approximate solution $\mathbf{w}_h(t,x)$ to $\mathbf{w}(t,x)$ such that for each time $t \in [0, t_{\max}]$, $\mathbf{w}_h(t,x)$ belongs to the finite dimensional space

$$V_h = \left\{ v \in L^1(I) : \ v|_{I_j} \in P^k(I_j), \ j = 0, 1, 2, \ldots .N \right\}, \tag{25}$$

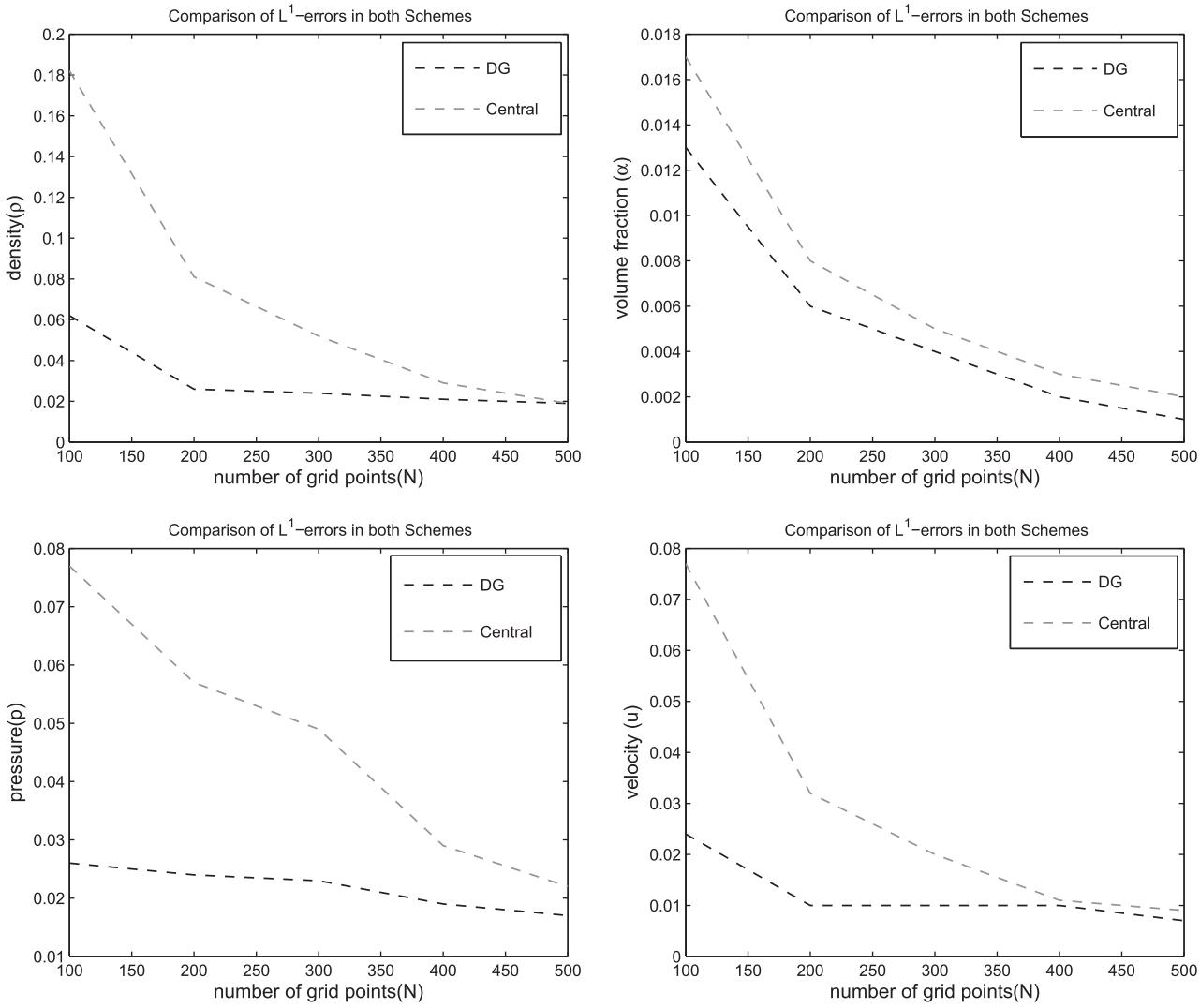

Fig. 3. Convergence study of DG and Central NT schemes for Problem 1. Comparison of L^1-errors of both schemes at different grid points.

where $P^k(I_j)$ represents the space of polynomials in I_j of degree at most k. Note that in V_h, the functions are allowed to have jumps at the cell interface $x_{j+\frac{1}{2}}$. To determine the approximate solution $\mathbf{w}_h(t,x)$, a weak formulation is needed which is usually obtained by multiplying Eq. (21) with a smooth function $v(x)$ and by integrating over the interval I_j. After using integration by parts, the weak formulation appears in the following form

$$\int_{I_j}\frac{\partial \mathbf{w}(t,x)}{\partial t}v(x)dx=\int_{I_j}\mathbf{f}(\mathbf{w}(t,x))\frac{\partial}{\partial x}v(x)dx+\int_{I_j}\mathbf{s}(\mathbf{w}(t,x))v(x)dx - \left[\mathbf{f}\left(\mathbf{w}\left(t,x_{j+\frac{1}{2}}\right)\right)v(x_{j+\frac{1}{2}})-\mathbf{f}\left(\mathbf{w}\left(t,x_{j-\frac{1}{2}}\right)\right)v(x_{j-\frac{1}{2}})\right]. \tag{26}$$

One way to apply Eq. (25) is to choose Legendre polynomials, $P_l(x)$, of order l as local basis functions. In this approach, the L^2-orthogonality property of Legendre polynomials can be exploited as expressed below

$$\int_{-1}^{1}P_l(s)P_{l'}(s)ds=\left(\frac{2}{2l+1}\right)\delta_{ll'}. \tag{27}$$

For each $x\in I_j$, the solution $\mathbf{w}_h$ can be expressed as

$$\mathbf{w}_h(t,x)=\sum_{l=0}^{k}\mathbf{w}_j^{(l)}\varphi_l(x), \tag{28}$$

where

$$\varphi_l(x)=P_l\big(2(x-x_j)/\Delta x_j\big). \tag{29}$$

It can be easily proved that

$$\left(\frac{1}{2l+1}\right)\mathbf{w}_j^{(l)}(t)=\frac{1}{\Delta x_j}\int_{I_j}\mathbf{w}_h(t,x)\varphi_l(x)dx. \tag{30}$$

Since the above Legendre polynomials are used as local basis functions, the smooth function $v(x)$ can be replaced by the test function $\varphi_l\in V_h$ and the exact solution $\mathbf{w}$ by the approximate solution $\mathbf{w}_h$. Moreover, the function $\mathbf{w}_{j+\frac{1}{2}}=\mathbf{w}\left(t,x_{j+\frac{1}{2}}\right)$ is not known at the cell interface $x_{j+\frac{1}{2}}$. Therefore, the flux $\mathbf{f}(\mathbf{w}(t,x))$ has to be approximated by a numerical flux that depends on two values of $\mathbf{w}_h(t,x)$, i.e.,

$$\mathbf{f}\left(\mathbf{w}\left(t,x_{j+\frac{1}{2}}\right)\right)\approx\mathbf{h}_{j+\frac{1}{2}}=\mathbf{h}\left(\mathbf{w}\left(t,x_{j+\frac{1}{2}}^{-}\right),\mathbf{w}\left(t,x_{j-\frac{1}{2}}^{+}\right)\right). \tag{31}$$

Here,

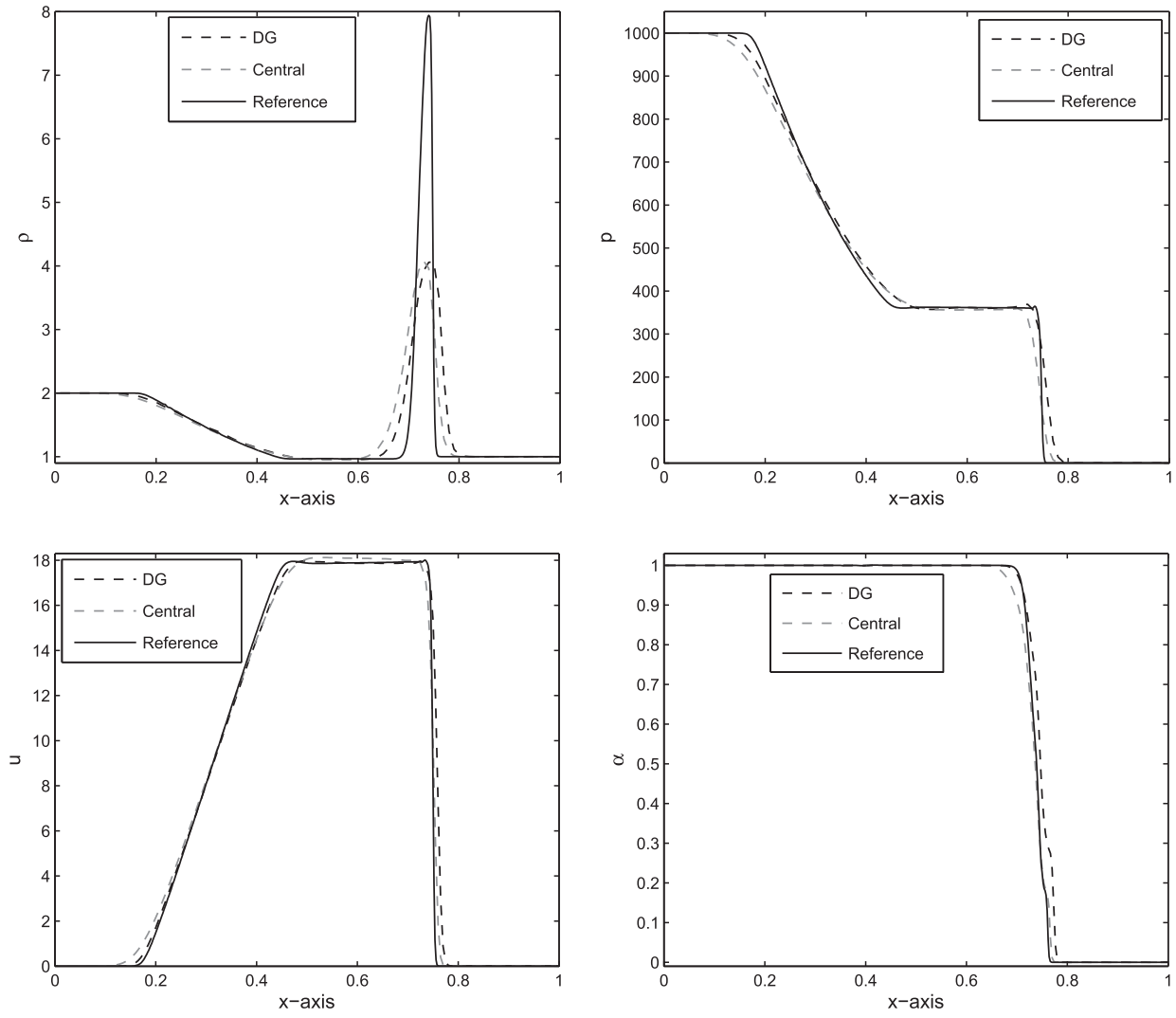

Fig. 4. Comparison of DG and central NT schemes for Problem 2 at time $t = 0.012$.

$$\mathbf{w}^{-}_{j+\frac{1}{2}} = \mathbf{w}_h\left(t, x^{-}_{j+\frac{1}{2}}\right) = \sum_{l=0}^{k} \mathbf{w}_j^{(l)} \varphi_l\left(x_{j+\frac{1}{2}}\right), \tag{32}$$

$$\mathbf{w}^{+}_{j-\frac{1}{2}} = \mathbf{w}_h\left(t, x^{+}_{j-\frac{1}{2}}\right) = \sum_{l=0}^{k} \mathbf{w}_j^{(l)} \varphi_l\left(x_{j-\frac{1}{2}}\right). \tag{33}$$

Using the above definitions, the weak formulation in Eq. (26) simplifies to

$$\begin{aligned}\frac{d\mathbf{w}_j^{(l)}(t)}{dt} = &-\frac{2l+1}{\Delta x_j}\left(\mathbf{h}_{j+\frac{1}{2}}\varphi_l\left(x_{j+\frac{1}{2}}\right) - \mathbf{h}_{j-\frac{1}{2}}\varphi_l\left(x_{j-\frac{1}{2}}\right)\right) + \frac{2l+1}{\Delta x_j} \\ &\times \int_{I_j}\left(\mathbf{f}(\mathbf{w}_h(t,x))\frac{d\varphi_l(x)}{dx}\right)dx + \frac{2l+1}{\Delta x_j} \\ &\times \int_{I_j} \mathbf{s}(\mathbf{w}_h(t,x))\varphi_l(x)dx.\end{aligned} \tag{34}$$

The first four terms of the source term are zero, while the integral for the fifth term containing sources of mechanical and thermodynamical works ($s_5 = s_5^M + s_5^T$) are expressed after some manipulation as

$$\begin{aligned}\int_{I_j} \mathbf{s}_5\varphi_l(x)dx = &\bar{u}\left[\alpha_{j+\frac{1}{2}}p_{j+\frac{1}{2}}\varphi_l\left(x_{j+\frac{1}{2}}\right) - \alpha_{j-\frac{1}{2}}p_{j-\frac{1}{2}}\varphi_l\left(x_{j-\frac{1}{2}}\right)\right] \\ &- \bar{u}\bar{\beta}\left[p_{j+\frac{1}{2}}\varphi_l\left(x_{j+\frac{1}{2}}\right) - p_{j-\frac{1}{2}}\varphi_l\left(x_{j-\frac{1}{2}}\right)\right] \\ &+ \bar{p}\bar{c}\bar{\alpha}(1-\bar{\alpha})\left[u_{j+\frac{1}{2}}\varphi_l\left(x_{j+\frac{1}{2}}\right) - u_{j-\frac{1}{2}}\varphi_l\left(x_{j-\frac{1}{2}}\right)\right] \\ &+ \bar{u}\int_{I_j}\left((\beta p - \alpha p)\frac{d\varphi_l(x)}{dx}\right)dx \\ &- \bar{p}\bar{c}\bar{\alpha}(1-\bar{\alpha})\int_{I_j}\left(u(t,x)\frac{d\varphi_l(x)}{dx}\right)dx.\end{aligned} \tag{35}$$

In the above equation, the bar terms represent the average values, for example for any $\bar{\psi}$, we have $\bar{\psi} = \frac{1}{2}(\psi_j + \psi_{j+1})$.

It remains to choose the appropriate numerical flux function h. The above equations define a monotone scheme if the numerical flux function $\mathbf{h}(a,b)$ is consistent, $\mathbf{h}(\mathbf{w},\mathbf{w}) = \mathbf{f}(\mathbf{w})$, and satisfies the Lipschitz continuity condition, i.e., $\mathbf{h}(a,b)$ is a non-decreasing function of its first argument and non-increasing function of its second argument [29,30]. The two following numerical flux functions are used that satisfy the above properties [29,30].

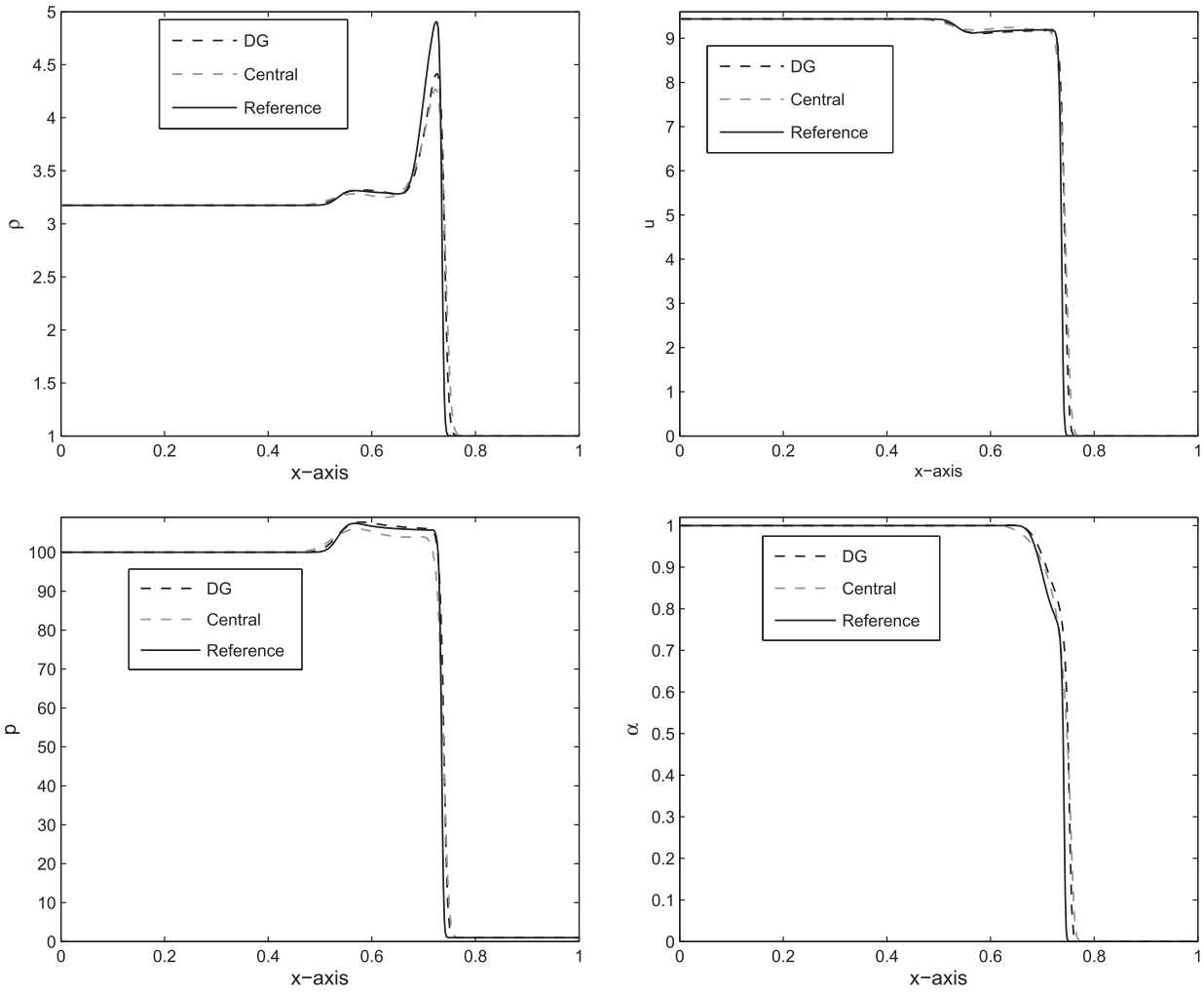

Fig. 5. Comparison of DG and central NT schemes for Problem 3 at time $t = 0.02$.

Table 2
Comparison of L^1-errors for Problem 4.

N	Density (ρ)		Volume fraction (α)		Pressure (p)		Velocity (u)	
	DG	Central	DG	Central	DG	Central	DG	Central
100	23.15	28.45	0.021	0.022	1.94×10^7	2.40×10^7	23.52	28.30
200	10.85	12.97	0.009	0.010	8.40×10^6	1.03×10^7	9.852	11.71
300	4.923	6.951	0.003	0.005	4.45×10^6	6.65×10^6	5.234	6.152
400	2.403	3.392	0.002	0.002	2.97×10^6	4.57×10^6	3.322	4.212
500	1.217	2.499	0.001	0.002	1.01×10^6	2.01×10^6	1.294	2.602

(i) The Lax-Friedrichs flux:

$$\mathbf{h}^{LF}(a,b) = \frac{1}{2}[\mathbf{f}(a) + \mathbf{f}(b) - C(b-a)], \tag{36}$$

$$C = \max_{\inf\ \mathbf{w}^{(0)}(x) \leqslant s \leqslant \sup\ \mathbf{w}^{(0)}(x)} |\mathbf{f}'(s)|. \tag{37}$$

(ii) The Local Lax-Friedrichs flux:

$$\mathbf{h}^{LLF}(a,b) = \frac{1}{2}[\mathbf{f}(a) + \mathbf{f}(b) - C(b-a)], \tag{38}$$

$$C = \max_{\min\ (a,b) \leqslant s \leqslant \max\ (a,b)} |\mathbf{f}'(s)|. \tag{39}$$

The Gauss-Lobatto quadrature formula of 10th order was used to numerically approximate the integral terms appearing on the right side of Eq. (34).

To achieve local maximum principle with respect to the means, some limiting procedure is needed. For that purpose, it is required to modify the interfaces values $\mathbf{w}^{\pm}_{j\pm\frac{1}{2}}$ in Eqs. (31)–(33) by some local projection limiter. At this end, Eqs. (32) and (33) can be written as [18–20]

$$\mathbf{w}^{-}_{j+\frac{1}{2}} = \mathbf{w}^{(0)}_j + \tilde{\mathbf{w}}_j, \quad \mathbf{w}^{+}_{j-\frac{1}{2}} = \mathbf{w}^{(0)}_j - \hat{\mathbf{w}}_j, \tag{40}$$

where

$$\tilde{\mathbf{w}}_j = \sum_{l=1}^{k} \mathbf{w}^{(l)}_j \varphi_l\left(x_{j+\frac{1}{2}}\right), \quad \hat{\mathbf{w}}_j = -\sum_{l=1}^{k} \mathbf{w}^{(l)}_j \varphi_l\left(x_{j-\frac{1}{2}}\right). \tag{41}$$

Next, $\tilde{\mathbf{w}}_j$ and $\hat{\mathbf{w}}_j$ can be modified as

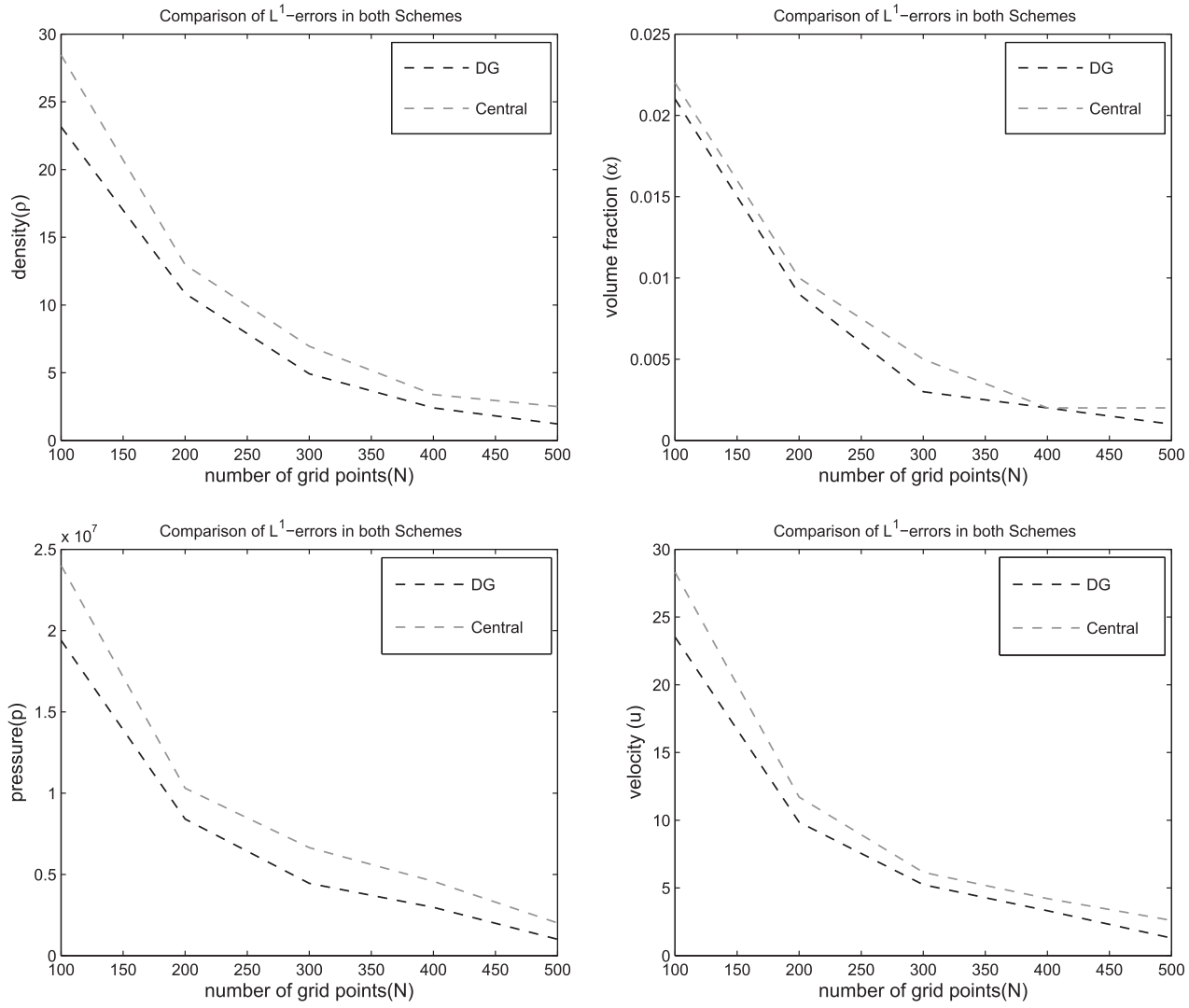

Fig. 6. Convergence study of DG and Central NT schemes for Problem 4. Comparison of L^1-errors of both schemes at different grid points.

$$\tilde{\mathbf{w}}_j^{(\mathrm{mod})} = \mathrm{mm}\left(\tilde{\mathbf{w}}_j, \Delta_+\mathbf{w}_j^{(0)}, \Delta_-\mathbf{w}_j^{(0)}\right), \tag{42}$$

$$\hat{\mathbf{w}}_j^{(\mathrm{mod})} = \mathrm{mm}\left(\hat{\mathbf{w}}_j, \Delta_+\mathbf{w}_j^{(0)}, \Delta_-\mathbf{w}_j^{(0)}\right), \tag{43}$$

where $\Delta_\pm\mathbf{w}_j = \pm(\mathbf{w}_{j\pm1} - \mathbf{w}_j)$ and mm is the usual minmod function which is defined as

$$\mathrm{mm}(a_1, a_2, a_3) = \begin{cases} s \cdot \min\limits_{1\leqslant i\leqslant 3}|a_i| & \text{if } \mathrm{sign}(a_1) = \mathrm{sign}(a_2) = \mathrm{sign}(a_3) = s \\ 0 & \text{otherwise.} \end{cases} \tag{44}$$

Then, Eq. (40) modifies to

$$\mathbf{w}_{j+\frac{1}{2}}^{-(\mathrm{mod})} = \mathbf{w}_j^{(0)} + \tilde{\mathbf{w}}_j^{(\mathrm{mod})}, \quad \mathbf{w}_{j-\frac{1}{2}}^{+(\mathrm{mod})} = \mathbf{w}_j^{(0)} - \hat{\mathbf{w}}_j^{(\mathrm{mod})}, \tag{45}$$

and Eq. (31) is replaced by

$$\mathbf{h}_{j+\frac{1}{2}} = \mathbf{h}\left(\mathbf{w}_{j+\frac{1}{2}}^{-(\mathrm{mod})}, \mathbf{w}_{j-\frac{1}{2}}^{+(\mathrm{mod})}\right). \tag{46}$$

This limiter corresponds to adding the minimum amount of numerical diffusion while preserving the stability of the scheme. The DG-method in addition to the above explained slope limiter has been proved to be stable [31].

Here, we have implemented the WENO limiter [32] to eliminate oscillations and enforce the stability. In this procedure, we firstly identify "troubled cells", namely those cells that need to be reconstructed. A troubled cell is the one for which the minmod functions given by Eqs. (42) and (43) gets active (i.e. returns other than the first argument) and is marked for further reconstructions. For the troubled cells, we would like to reconstruct the polynomial solution while retaining its cell average.

Finally, a Runge-Kutta method is implemented that maintains the TVB property of the method is needed to solve the resulting system of ODE. Let us rewrite Eq. (34) in a concise form as

$$\frac{d\mathbf{w}_h}{dt} = L_h(t, \mathbf{w}_h). \tag{47}$$

Then, the r-order TVB Runge-Kutta method can be used to approximate Eq. (47)

$$\mathbf{w}_h^{(k)} = \sum_{l=0}^{k-1}\left[\alpha_{kl}\mathbf{w}_h^{(l)} + \beta_{kl}\Delta t L_h(t^n + d_l\Delta t, \mathbf{w}_h^{(l)})\right], \quad k = 1, 2, \ldots, r, \tag{48}$$

were based on the boundary conditions

$$\mathbf{w}_h^{(0)} = \mathbf{w}_h^n, \quad \mathbf{w}_h^{(r)} = \mathbf{w}_h^{n+1}. \tag{49}$$

For the second order TVB Runge-Kutta method the coefficient are given as [18]

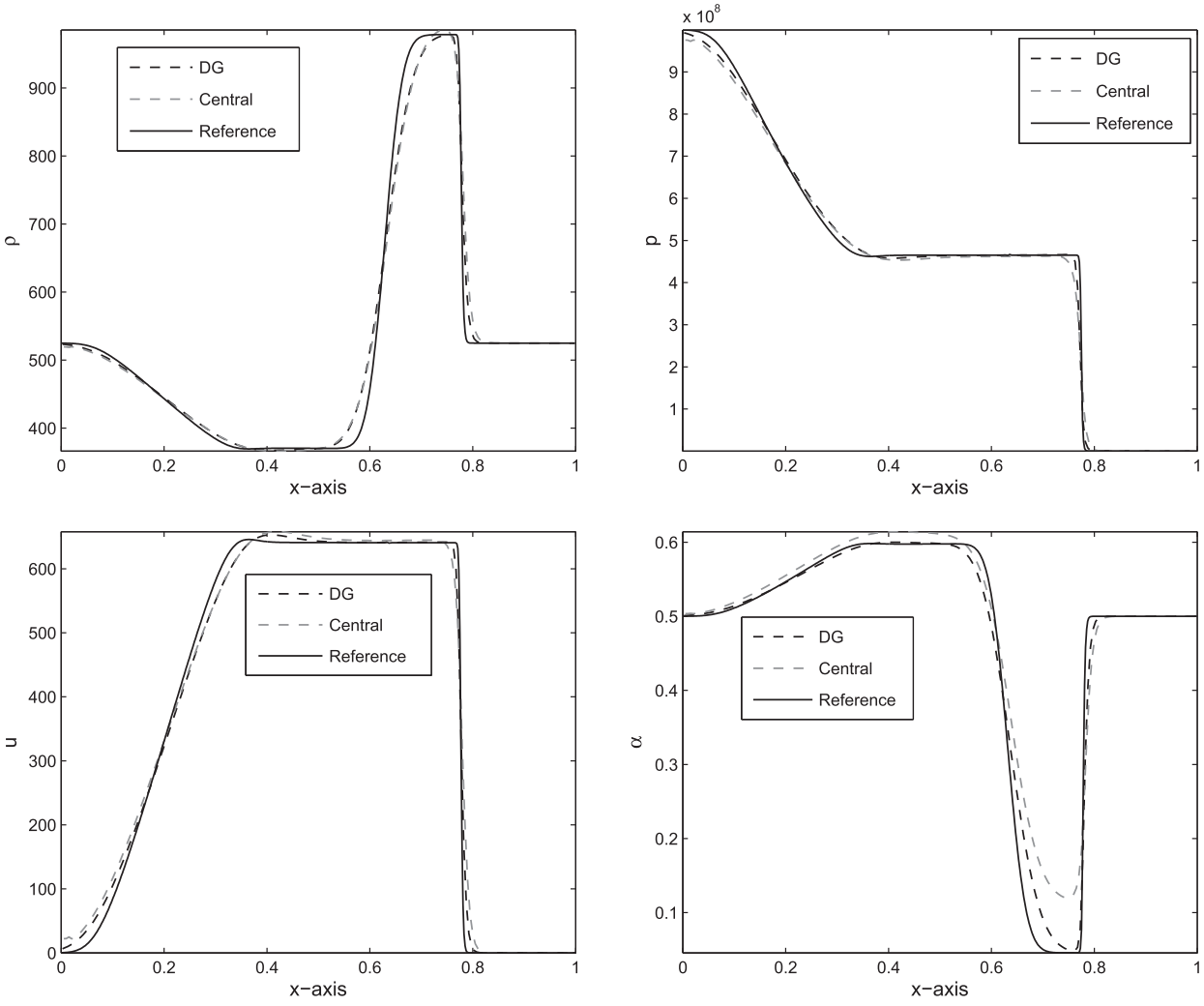

Fig. 7. Comparison of DG and central NT schemes for Problem 4 at time $t = 200$ μs.

$$\alpha_{10} = \beta_{10} = 1, \quad \alpha_{20} = \alpha_{21} = \beta_{21} = \frac{1}{2}, \quad \beta_{20} = 0; \quad d_0 = 0, \quad d_1 = 1. \tag{50}$$

While, for the third order TVB Runge-Kutta method the coefficient are given as

$$\alpha_{10} = \beta_{10} = 1, \quad \alpha_{20} = \frac{3}{4}, \quad \beta_{20} = 0, \quad \alpha_{21} = \beta_{21} = \frac{1}{4}, \quad \alpha_{30} = \frac{1}{3},$$
$$\beta_{30} = \alpha_{31} = \beta_{31} = 0, \quad \alpha_{32} = \beta_{32} = \frac{2}{3}, \quad d_0 = 0, \quad d_1 = 1, \quad d_2 = \frac{1}{2}. \tag{51}$$

In order to guarantee numerical convergence and stability of the DG-scheme, the time step is taken according to the following Courant-Friedrichs-Lewy (CFL) condition [18,29]

$$\Delta t \leqslant \left(\frac{1}{2k+1}\right)\frac{\min(\Delta x_j)}{\lambda_{max}}, \tag{52}$$

where λ_{max} is the maximum eigenvalue of the Jacobian matrix $\frac{\partial \mathbf{f}(\mathbf{w})}{\partial \mathbf{w}}$, and $k = 1, 2$ for the second and third order schemes, respectively. This time step is adaptive which reduces for the case of large variations (large slopes) in the solution and increases otherwise.

Numerical test problems

In this section, six one-dimensional test problems are considered to verify the efficiency and accuracy of the proposed schemes.

Problem 1 (*Sod's problem*). The Sod's problem [6,33,34] is the well known test problem in the single phase gas dynamics. In this problem, gases are separated by a very thin membrane placed at $x = 0.5$ and are initially at rest. The left side gas has high density and pressure as compared to right side gas. After removing the membrane, the gases evolution in time take place. The initial data for the problem are given as

$$(\rho, u, p, \alpha) = (10, 0, 10, 1), \quad \text{if } x \leqslant 0.5, \tag{53}$$
$$(\rho, u, p, \alpha) = (0.125, 0, 0.1, 0), \quad \text{if } x > 0.5. \tag{54}$$

The ratio of specific heats for the left and right side gases are taken as $\gamma_L = 1.4$ and $\gamma_R = 1.6$, respectively. In Fig. 3, the solutions of discontinuous Galerkin and central NT schemes are compared at 100 mesh cells at $t = 0.15$. The reference solution is obtained from the discontinuous Galerkin scheme at 500 grid points. We can observe a left-going rarefaction wave, a right-going shock wave and a right-moving two-fluid interface in the solution. Both schemes give correct location of the shocks and have comparable accuracy. Moreover, no pressure oscillations are observed in the solution. This problem is considered to check the accuracy of DG and central NT schemes. The results for the errors in density and volume fraction are computed and depicted in the form of plots in Fig. 2. The L^1-errors for both schemes are calculated and displayed in Table 1. From the table and plots one can easily observe

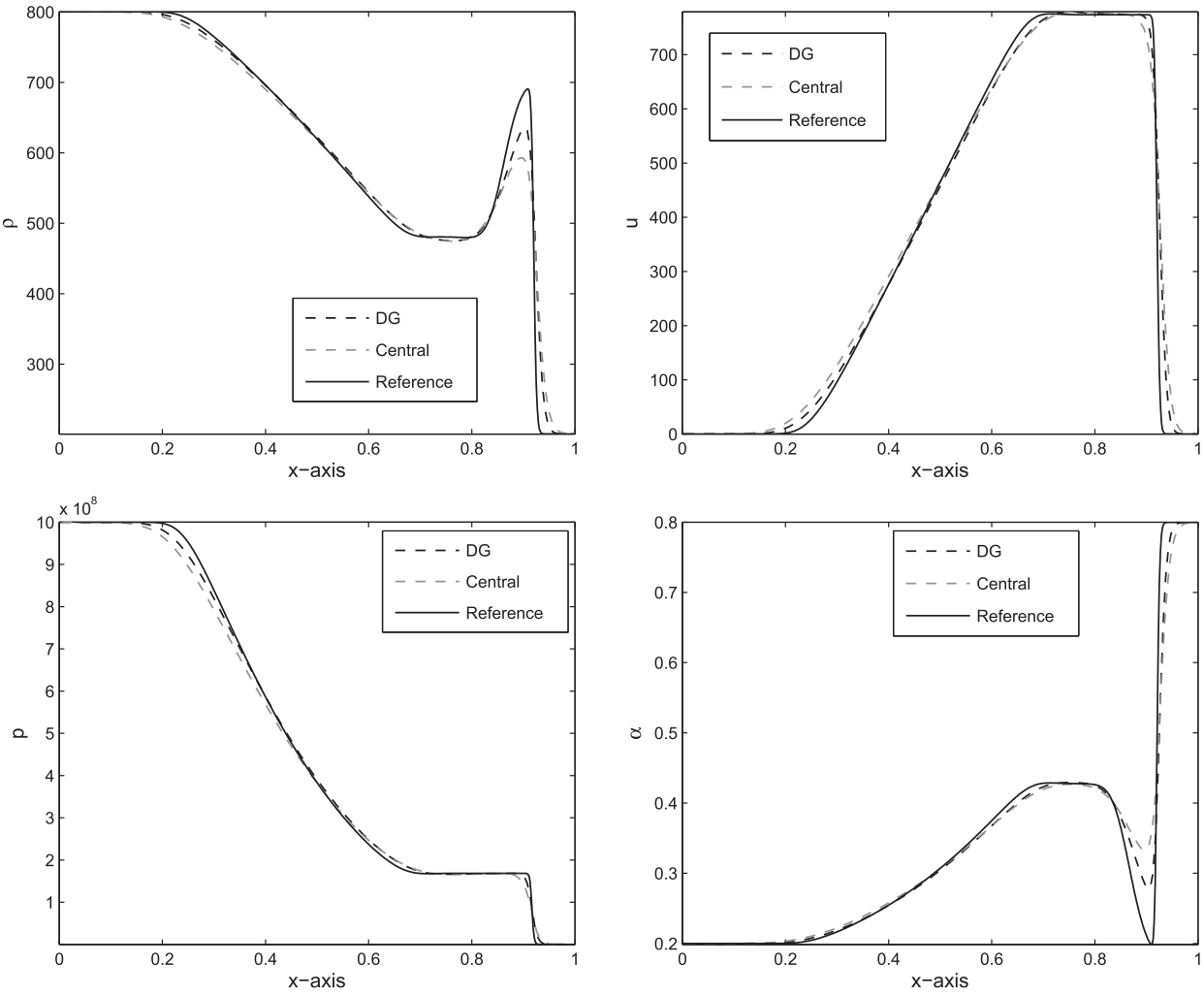

Fig. 8. Comparison of DG and central NT schemes for Problem 5 at time $t = 200$ μs.

that DG scheme produces less errors in density, volume fraction, pressure and velocity as compared to the central NT scheme. The L^1-errors of both schemes are functions of number of grid points that can be seen in the plots of Fig. 2 and Table 1.

Problem 2 (*Two-fluid mixture problem*). The initial data are given as

$$(\rho, u, p, \alpha) = (2.0, 0, 1000, 1), \quad \text{if } x \leqslant 0.5, \tag{55}$$
$$(\rho, u, p, \alpha) = (1, 0, 0.01, 0), \quad \text{if } x > 0.5. \tag{56}$$

Here, $\gamma_L = 1.4$ and $\gamma_R = 1.2$, $\Pi_L = 0 = \Pi_R$, and CFL = 0.5. This problem was also considered in [6,33,34]. It is a hard test problem for a numerical scheme. From the solution we can see a left moving rarefaction wave, a contact discontinuity, and a right moving shock wave. The right moving shock hits the interface at $x = 0.5$. The shock continues to move towards right and a rarefaction wave is created which is moving towards left. The results of discontinuous Galerkin method and central NT scheme are given on 100 mesh cells and the final simulation time is taken as $t = 0.012$. The numerical solutions are presented in Fig. 4. Both of the schemes give comparable results. However, it can be noticed that discontinuous Galerkin scheme gives better resolution of peaks and sharp discontinuities. For the considered 200 grid points, the L^1-errors of DG and NT central schemes in the density are 0.083, 0.115, in the volume fraction are 0.013, 0.0163, in the pressure are 4.727, 7.618, and in the velocity are 0.163, 0.241, respectively. These errors further verify the better accuracy of our proposed numerical scheme.

Problem 3 (*No-reflection problem*). The initial data are given as

$$(\rho, u, p, \alpha) = (3.1748, 9.435, 100, 1), \quad \text{if } x \leqslant 0.5, \tag{57}$$
$$(\rho, u, p, \alpha) = (1, 0, 1, 0), \quad \text{if } x > 0.5. \tag{58}$$

The ratios for the specific heats are considered as $\gamma_L = 1.667$ and $\gamma_R = 1.2$. Moreover, $\Pi_L = 0 = \Pi_R$ and CFL = 0.4 are taken as. We discretize the computational domain $[0, 1]$ into 100 mesh cells and the final simulation time is $t = 0.02$. This is a hard test problem for a numerical scheme due to large jumps in pressure at the interface. The choice of pressure and velocity jump over the shock prevents the creation of a reflection wave. Therefore, a shock wave moves to the right. The results are depicted in Fig. 5. Wiggles can be seen in the velocity and pressure plots of both schemes, representing small waves that are reflected to the left. However, unlike real velocity and pressure oscillations, these wiggles reduces on refined meshes. Similar type of wiggles are also reported in the results of [6,33,34]. For the considered 200 grid points, the L^1-errors of DG and NT central schemes in the density are 0.046, 0.065, in the volume fraction are 0.015, 0.021, in the pressure are 0.741, 1.071, and in the velocity are 0.074, 0.108, respectively.

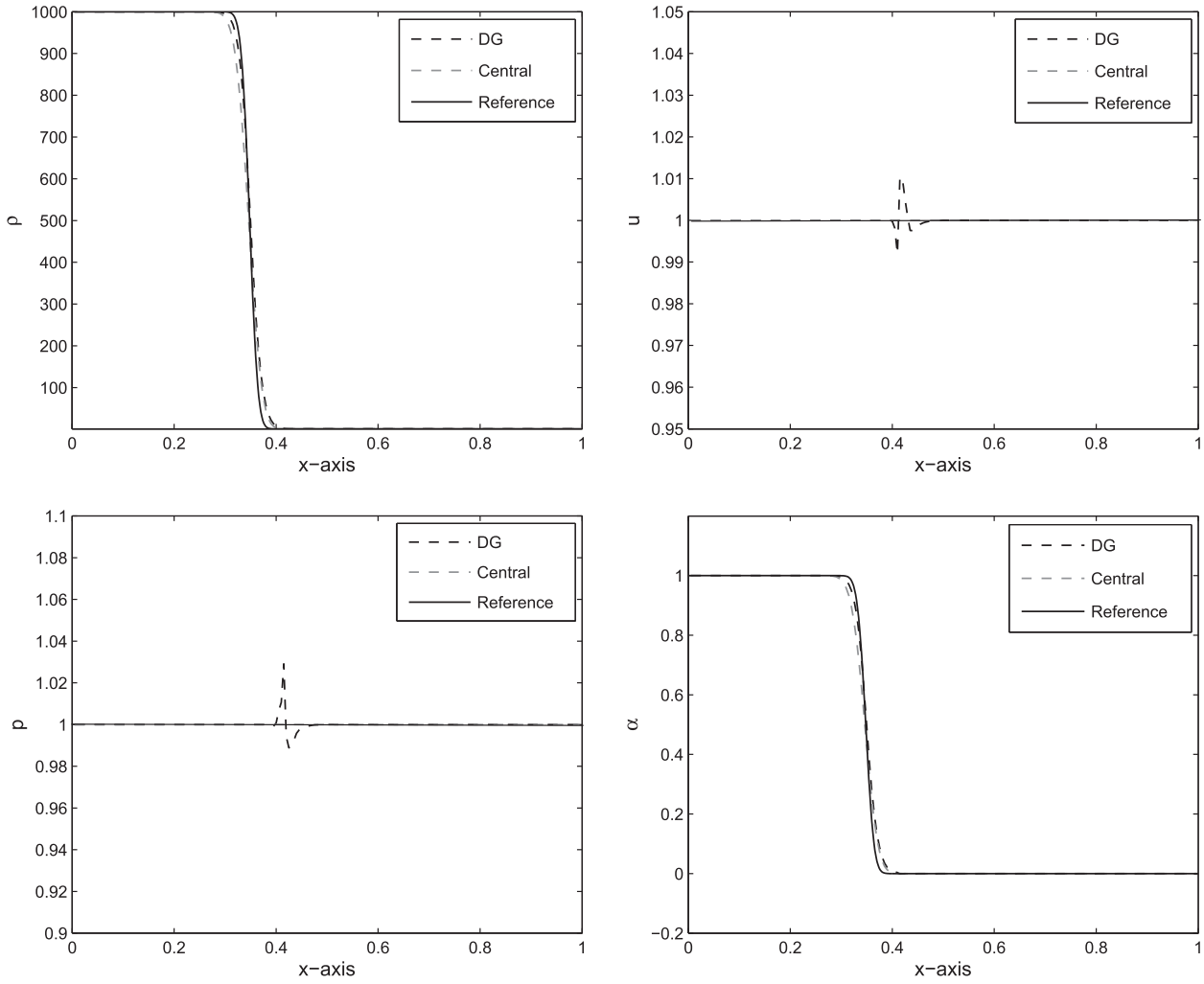

Fig. 9. Comparison of DG and central NT schemes for Problem 6 at time $t = 0.1$.

These errors further verify the better accuracy of our proposed numerical scheme.

Problem 4 (*Water-air mixture problem*). This one-dimensional problem corresponds to the water-air mixture [6,7,33,34]. The initial data are given as

$$(\rho, u, p, \alpha) = (525, 0, 10^9, 0.5), \quad \text{if } x \leqslant 0.5, \tag{59}$$
$$(\rho, u, p, \alpha) = (525, 0, 10^5, 0.5), \quad \text{if } x > 0.5. \tag{60}$$

Here, $\gamma_L = 1.4$, $\gamma_R = 4.4$, $\Pi_L = 0$, $\Pi_R = 6 \times 10^8$ and CFL = 0.5. The computational domain of the problem $[0, 1]$ is divided into 100 mesh cells and the final simulation time is $t = 200$ μs. The numerical results are shown in Fig. 7. Although the initial composition of the mixture is constant, it evolves in space and time. It can be observed that both schemes give comparable results. Moreover, our results are in good agreement with the results in [7]. The L^1-errors for both schemes are calculated and displayed in Table 2, also the plots for the errors are drawn and depicted in Fig. 6. From the table and plots one can easily observe that DG scheme produces less errors in density, volume fraction, pressure and velocity as compared to the central NT scheme with the increase in number of grid points. In both schemes the L^1-errors are functions of number of grid points that can be seen from the graphs.

Problem 5 (*Water-air mixture problem*). Again a one-dimensional water-air mixture problem [6,7,33,34] is considered. However, this problem differs from the previous water-air problem by allowing changes in the mixture composition. The initial data are given as

$$(\rho, u, p, \alpha) = (1, 0, 10^9, 0.2), \quad \text{if } x \leqslant 0.7, \tag{61}$$
$$(\rho, u, p, \alpha) = (10^3, 0, 10^5, 0.8), \quad \text{if } x > 0.7. \tag{62}$$

Here, $\gamma_L = 1.4$, $\gamma_R = 4.4$, $\Pi_L = 0$, $\Pi_R = 6 \times 10^8$ and $CFL = 0.5$. The numerical results are obtained on 100 mesh cells and the final simulation time is $t = 200$ μs. The numerical results are shown in Fig. 8. In this figure it can be noted that discontinuous Galerkin method gives comparable results to the central NT scheme. Moreover, the numerical results are in good agreement with those published in [7]. For the considered 200 grid points, the L^1-errors of DG and NT central schemes in the density are 609.8, 615.3, in the volume fraction are 0.659, 0.660, in the pressure are 4.87×10^8, 4.97×10^8 and in the velocity are 360.8, 366.5, respectively. These errors further verify the better accuracy of our proposed numerical scheme.

Problem 6 (*Translating two-fluid interface*). The initial data for the problem are given as

$$(\rho, u, p, \alpha) = (1000, 1, 1, 1), \quad \text{if } x \leqslant 0.25, \tag{63}$$
$$(\rho, u, p, \alpha) = (1, 1, 1, 0), \quad \text{if } x > 0.25. \tag{64}$$

The ratios for the specific heats are given as $\gamma_L = 1.4$ and $\gamma_R = 1.6$. We have chosen 100 mesh cells for numerical solution and the final simulation time is $t = 0.1$. This problem is a contact discontinuity of water-air density ratio. The numerical results are shown in Fig. 9. The same problem was also considered in [6,33,34]. In this problem, both pressure and velocity are the same. Therefore, the interface is moving to the right with uniform speed and pressure. The numerical results show that discontinuous Galerkin method resolves the two-fluid interface very well as compared to the central scheme. Moreover, both velocity and pressure profiles are oscillation free. For the considered 200 grid points, the L^1-errors of DG and NT central schemes in the density are 7.013, 8.788, in the volume fraction are 0.007, 0.008, in the pressure are 0.0, 0.0, and in the velocity are 0.0, 0.0, respectively. These errors further verify the better accuracy of our proposed numerical scheme.

Conclusions

A TVB Runge-Kutta DG finite element method was extended to solve the compressible two-phase five-equation model. It was observed that the proposed scheme is capable to accurately capture sharp discontinuities and avoids excessive numerical diffusion or spurious oscillations. To preserve the positivity of the scheme a WENO limiter was used. To achieve the second order accuracy in time a TVB Runge-Kutta method was utilized. The numerical results obtained show that the considered five-equation model capable to study dynamics of two-phase flows. For validation, the results of proposed numerical scheme are compared qualitatively and quantitatively with those of staggered central scheme and those available in the literature. Good agreements were found in the results of both schemes. However, it was found that DG-method produces less errors in the solutions and better resolves the sharp discontinuities in the solutions. The DG-method was for the first time applied to successfully approximate the considered two-phase flow model containing the non-conservative source term.

Appendix A. Supplementary data

Supplementary data associated with this article can be found, in the online version, at https://doi.org/10.1016/j.rinp.2017.12.044.

References

[1] Ishii M. Thermo-fluid dynamic theory of two-phase flow. Paris: Eyrolles; 1975.
[2] Baer MR, Nunziato JW. A two-phase mixture theory for the deflagration-to-detonation transition (DDT) in reactive granular materials. Int J Multiphase Flows 1986;12:861–89.
[3] Abgrall R, Saurel R. Discrete equations for physical and numerical compressible multiphase mixtures. J Comput Phys 2003;186:361–96.
[4] Saurel R, Abgrall R. A multiphase Godunov method for compressible multifluids and multiphase flows. J Comput Phys 1999;150:425–67.
[5] Kapila AK, Menikoff R, Bdzil JB, Son SF, Stewart DS. Two-phase modeling of deflagration-to-detonation transition in granular materials. Phys Fluids 2001;10:3002–24.
[6] Kreeft JJ, Koren B. A new formulation of Kapila's five-equation model for compressible two-fluid flow, and its numerical treatment. J Comput Phys 2010;229:6220–42.
[7] Murrone A, Guillard H. A five-equation reduced model for compressible two phase flow problems. J Comput Phys 2002;202:664–98.
[8] Wood AB. A textbook of sound. London: Bell Sons Ltd.; 1930.
[9] Caleffi V, Valiani A, Bernini A. Fourth-order balanced source term treatment in central WENO schemes for shallow water equations. J Comp Phys 2006;218:228–45.
[10] Castro MJ, Maćýas J, Pares C. A Q-scheme for a class of systems of coupled conservation laws with source term. Application to a two-layer 1-D shallow water system. ESAIM, M2AN 2001;35:107–27.
[11] Qamar S, Mudasser S. On the application of a variant CESE method for solving two-dimensional ideal MHD equations. Appl Numer Math 2010;60:587–606.
[12] Tao T, Xu K. Gas-kinetic schemes for the compressible Euler equations: positivity-preserving analysis. Zeitschrift für angewandte Mathematik und Physik ZAMP 1999;50:258–81.
[13] Xing Y, Shu C-W. High order finite difference WENO schemes with the exact conservation property for the shallow water equations. J Comput Phys 2005;208:206–27.
[14] Ansari MR, Daramizadeh A. Numerical simulation of compressile two-phase flow using a diffuse interface method. Int J Heat Fluid Flow 2013;42:209–23.
[15] Henry de Frahan MT, Sreenivas V, Eric J. A new limiting procedure for discontinuous Galerkin methods applied to compressible multiphase flows with shocks and interfaces. J Comput Phys 2015;280:489–509.
[16] Coralic V, Colonius T. Finite-volume WENO scheme for viscous compressible multicomponent flows. J Comput Phys 2014;274:95–121.
[17] Reed WH, Hill TR. Triangular mesh methods for the neutron transport equation. Los Alamos Scientific Laboratory Report LA-UR; 1973:73–9.
[18] Cockburn B, Shu C-W. TVB Runge-Kutta local projection discontinuous Galerkin finite element method for conservation laws II, General framework. Math Comput 1989;52:411–35.
[19] Cockburn B, Lin S-Y. TVB Runge-Kutta local projection discontinuous Galerkin finite element method for conservation laws III: one-dimensional systems. J Comput Phys 1989;84:90–113.
[20] Cockburn B, Shu C-W. Runge Kutta discontinuous Galerkin methods for convection-dominated problems. J Sci Comput 2001;16:173–261.
[21] Chen Z, Cockburn B, Jerome J, Shu CW. Mixed-RKDG finite element methods for the 2-D hydrodynamic model for semiconductor device simulation. VLSI Des 1995;3:145–58.
[22] Bassi F, Rebay S. A high-order accurate discontinuous finite element method for the numerical solution of the compressible Navier-Stokes equations. J Comput Phys 1997;131:267–79.
[23] Bahhar A, Baranger J, Sandri D. Galerkin discontinuous approximation of the transport equation and viscoelastic fluid flow on quadrilaterals. Numer Methods Partial Differ Equ 1998;14:97–114.
[24] Aizinger V, Dawson C, Cockburn B, Castillo P. Local discontinuous Galerkin method for contaminant transport. Adv Water Res 2000;24:73–87.
[25] Cockburn B, Dawson C. Approximation of the velocity by coupling discontinuous Galerkin and mixed finite element methods for flow problems. Comput Geosci 2002;6:502–22.
[26] Nessyahu H, Tadmor E. Non-oscillatory central differencing for hyperbolic conservation laws. SIAM J Comput Phys 1990;87:408–48.
[27] Hesthaven JS, Warburton T. Nodal discontinuous Galerkin methods, algorithms, analysis, and applications. Springer texts in applied mathematics, 54. New York: Springer Verlag; 2008.
[28] Qiu JX, Khoo BC, Shu C-W. A numerical study for the performance of the Runge-Kutta discontinuous Galerkin method based on different numerical fluxes. J Comput Phys 2006;212:540–65.
[29] Leveque RJ. Finite volume methods for hyperbolic systems. Cambridge University Press; 2003.
[30] Zhang P, Liu R-X. Hyperbolic conservation laws with space-dependent fluxes: II. General study of numerical fluxes. J Comput Appl Math 2005;176:105–29.
[31] Gowda V, Jaffr JA. A discontinuous finite element method for scalar nonlinear conservation laws. Rapport de recherche INRIA 1993;1848.
[32] Shu C-W. Essentially non-oscillatory and weighted essentially non-oscillatory schemes for hyperbolic conservation laws, NASA/CR-97-206253 ICASE Report No. 97-65; 1997.
[33] Ahmed M, Saleem MR, Zia S, Qamar S. Central upwind scheme for a compressible two phase flow model. PLoS One 2015;10:e0126273.
[34] Qamar S, Ahmed M. A high order kinetic-flux-vector splitting method for reduced five-equation model of compressible two-phase flows. J Comput Phys 2009;228:9059–78.